Therapeutics, Targets, and Chemical Biology

Cancer Research

ATM Deficiency Generating Genomic Instability Sensitizes Pancreatic Ductal Adenocarcinoma Cells to Therapy-Induced DNA Damage

Lukas Perkhofer[1], Anna Schmitt[2], Maria Carolina Romero Carrasco[1], Michaela Ihle[3], Stephanie Hampp[3], Dietrich Alexander Ruess[4], Elisabeth Hessmann[5], Ronan Russell[6], André Lechel[1], Ninel Azoitei[1], Qiong Lin[7], Stefan Liebau[8], Meike Hohwieler[1], Hanibal Bohnenberger[9], Marina Lesina[4], Hana Algül[4], Laura Gieldon[10], Evelin Schröck[10], Jochen Gaedcke[11], Martin Wagner[1], Lisa Wiesmüller[3], Bence Sipos[12], Thomas Seufferlein[1], Hans Christian Reinhardt[2], Pierre-Olivier Frappart[1], and Alexander Kleger[1]

Abstract

Pancreatic ductal adenocarcinomas (PDAC) harbor recurrent functional mutations of the master DNA damage response kinase ATM, which has been shown to accelerate tumorigenesis and epithelial–mesenchymal transition. To study how ATM deficiency affects genome integrity in this setting, we evaluated the molecular and functional effects of conditional *Atm* deletion in a mouse model of PDAC. ATM deficiency was associated with increased mitotic defects, recurrent genomic rearrangements, and deregulated DNA integrity checkpoints, reminiscent of human PDAC. We hypothesized that altered genome integrity might allow synthetic lethality-based options for targeted therapeutic intervention. Supporting this possibility, we found that the PARP inhibitor olaparib or ATR inhibitors reduced the viability of PDAC cells *in vitro* and *in vivo* associated with a genotype-selective increase in apoptosis. Overall, our results offered a preclinical mechanistic rationale for the use of PARP and ATR inhibitors to improve treatment of ATM-mutant PDAC. *Cancer Res; 77(20); 5576–90. ©2017 AACR.*

Introduction

Despite intensive basic and clinical research, deaths due to pancreatic ductal adenocarcinoma (PDAC) rank fourth among cancer-related mortality in the Western world, with an overall 5-year survival rate of only 4%. Recent predictions state that PDAC will be the second most cancer-related cause of death by 2030 (1). Genome sequencing studies have shed light on the mutational landscape of PDAC (2). Here, a small set of key driver mutations, such as *KRAS, TP53, CDKN2A*, or *SMAD4* have been identified along with a tremendously high number of passenger mutations, the latter establishing the strong intra- and intertumoral heterogeneity of PDAC. The current model of pancreatic carcinogenesis suggests that acinar-to-ductal metaplasia (ADM) is followed by acinar-to-ductal reprogramming (ADR), which step-wise progress to the more advanced precursor lesions, namely pancreatic intraepithelial neoplasias (PanIN) to form frank PDAC. Interestingly, the mutational landscape of advanced PanINs already share around 66% of the mutations present in established PDAC (3). A recent study discovered that single mitotic errors and significant genomic rearrangement can lead to rapid, synchronous clonogenic escape and metastatic disease (4). A key event seems to be chromothripsis, which is defined by extensive rearrangements confined to a single chromosome or to local regions of a few chromosomes. The latter can lead to the simultaneous knockout of several tumor suppressors. Thus, reasonable genetic mouse models need to faithfully reflect this dramatically altered genome integrity in human PDAC.

A subset of PDACs occurs in families with at least two affected first-degree relatives, and these are designated familial pancreatic

[1]Department of Internal Medicine I, University Hospital Ulm, Ulm, Germany. [2]Department of Internal Medicine, Division I, Hematology/Oncology, Clinical and Molecular Oncology, University Hospital Cologne, Cologne, Germany. [3]Division of Gynaecological Oncology, Department of Obstetrics and Gynaecology, University of Ulm, Ulm, Germany. [4]Klinik und Poliklinik für Innere Medizin II, Technische Universitaet Muenchen, Munich, Germany. [5]Department of Gastroenterology and Gastrointestinal Oncology, University Medical Center Goettingen, Goettingen, Germany. [6]Diabetes Centre, Department of Medicine, University of California at San Francisco, San Francisco, California. [7]Medical Faculty, Department of Cell Biology, Institute for Biomedical Engineering, RWTH Aachen University, Aachen, Germany. [8]Institute of Neuroanatomy, Eberhard Karls University Tuebingen, Tuebingen, Germany. [9]Department of Pathology, University Medical Center Goettingen, Goettingen, Germany. [10]Institut fuer Klinische Genetik, Medizinische Fakultaet Carl Gustav Carus, Technische Universitaet Dresden, Dresden, Germany. [11]Department of General, Visceral and Pediatric Surgery, University Medical Center Goettingen, Goettingen, Germany. [12]Department of Pathology and Neuropathology, University Hospital Tuebingen, Tuebingen, Germany.

Note: Supplementary data for this article are available at Cancer Research Online (http://cancerres.aacrjournals.org/).

L. Perkhofer and A. Schmitt contributed equally to this article.

P.-O. Frappart and A. Kleger jointly supervised this work and contributed equally to it.

Corresponding Authors: Alexander Kleger, Department of Internal Medicine I, University Hospital Ulm, Albert-Einstein-Allee 23, Ulm 89081, Germany. Phone: 49-1733492373; Fax: 49-73150044665; E-mail: alexander.kleger@uni-ulm.de; and Pierre-Olivier Frappart, Department of Internal Medicine I, University Hospital Ulm, Albert-Einstein-Allee 23, Ulm 89081, Germany. Phone: 49-73144823; Fax: 49-73150044665; E-mail: pierre.olivier.frappart@uni-ulm.de

doi: 10.1158/0008-5472.CAN-17-0634

AACR

cancers (FPC). In approximately 20% of the FPCs, inheritance has been attributed to a set of gene mutations leading to defects not only in classical PDAC driver genes (e.g., *CDKN2A*), but also in DNA repair genes, such as *BRCA1*, *BRCA2*, *ATM*, and *PALPB2* (5). Of note, the latter defects also refine the so-called "unstable" PDAC subtype. Here, at least *BRCA1/2*-mutant PDACs appear to be more sensitive toward platinum-based chemotherapy (2). However, genotype-tailored therapies for other genotypes than BRCA1/2-mutated PDACs, such as *ATM*-mutant cases, are still missing, and molecular phenotypes upon ATM loss need to be thoroughly characterized (2).

ATM is a serine/threonine protein kinase that phosphorylates many key proteins of the cell-cycle arrest, DNA repair, and apoptosis (6). In classical terms, ATM is recruited and activated by DNA double-strand breaks (DSB), thereby playing a central role in the DNA damage response (DDR; ref. 7). A recent study from our laboratory identified *ATM* mutations in 9% to 18% of PDACs, averaging 12% in large datasets of sporadic PDAC (8). Utilizing a genetically engineered mouse model of PDAC with *Atm* deletion, we found accelerated progression of PDAC with impaired NODAL- and BMP signaling resulting in more PanIN lesions at early stages. This accelerated cancer program coincided with enhanced stemness and epithelial-to-mesenchymal transition (EMT; ref. 8). Nevertheless, the consequences of *Atm* deletion on genome integrity in this model remain to be explored.

Here, we present that *Atm* deletion causes PDAC genome instability in our model and thereby sensitizes these cancers to therapeutically aggravated DNA damage. This approach has the capacity to establish a novel tailored approach for ATM low expressing human PDAC patients.

Materials and Methods

Ethics statement

All animal care and procedures followed German legal regulations and were previously approved by the governmental review board of the state of Baden-Württemberg, Bavaria, and North Rhine-Westphalia. All the aspects of the mouse work were carried out following strict guidelines to insure careful, consistent, and ethical handling of mice.

Mouse strain

The *LSL-Kras*^{G12D} (B6;129S4-*Kras*^{Tm4Tyj}/J), *Atm* Floxed (129-*Atm*$^{tm2.1Fwa}$/J), *Ptf1a-Cre* (B6;129-*Ptf1a*$^{tm1.1(CRE)Cvw}$) strains were as described in ref. 8. The mouse strains used are the following: KC: *LSL-Kras*^{G12D}, *Ptf1a-Cre*$^{+/-}$; AKC: *Atm*$^{F/F}$, *LSL-Kras*^{G12D}, *Ptf1a-Cre*$^{+/-}$.

Heterotopic model

For the heterotopic experiment, 10^6 tumor cells were resuspended in 100 μL serum-free DMEM medium and injected subcutaneously into 8- to 12-week-old RJ:NMRI-FOXN1 NU male mice (Janvier Labs). Mice were anesthetized (2.5% isoflurane) before injection. Upon formation of palpable subcutaneous tumors (200–300 mm^3 tumor volume), mice were treated with either vehicle solution, olaparib/VE-822, gemcitabine, or with olaparib/VE-822 plus gemcitabine. Tumor size was monitored every second day by measurement of perpendicular diameters with an external caliper and calculated by a modified ellipsoid formula $V = 0.5 \times (\text{length} \times \text{width}^2)$. Tumor volumes were measured on day 10 and 24 by μCT imaging (Aloka, Latheta LCT-100) and assessed by using the OsiriX and DICOM viewer software packages (OsiriX v.8.2, Pixmeo). Mice were sacrificed after 14 days of therapy.

Orthotopic model

For the orthotopic experiment, SCID mice were anesthetized (2.5% isoflurane) and injected into the tail of the pancreas with 10^6 tumor cells resuspended in PBS. The mice were maintained under analgesia for 48 hours after the operation. Tumor assessment was done by MRI scan on day 11, 18, and 25 posttransplantation and assessed by using the OsiriX and DICOM viewer software packages (OsiriX v.8.2, Pixmeo).

Tumor cell isolation and cell lines

Freshly isolated mouse PDAC was digested with collagenase D (Sigma-Aldrich). The cells were then trypsinized and passed through a 40-μm cell strainer before being cultured in DMEM (Sigma-Aldrich) supplied with 10% FCS and penicillin/streptomycin (Invitrogen). This stage was considered to be passage 0. Three KC cell lines, KC850, KC6059, and KC8878 and four AKC cell lines, AKC995, AKC5615, AKC5980, and AKC5982 were used throughout all the experiments. All the cell lines were isolated by ourselves between 2015 and 2017 and maintained frozen in liquid nitrogen. They were regularly controlled for their genotype and mycoplasma status. The cell lines were authenticated by parallel characterization in comparison with the pancreatic tissue by using different ductal markers and array comparative genomic hybridization (aCGH). The experiments were performed between passage 5 and 8. Mycoplasma tests were performed on these cell lines using the Mycoprobe Mycoplasma Detection Kit (R&D Systems, CUL001B) and all were negative.

Immunohistochemistry

IHC was performed on 5-μm paraffin sections. IHC was done according to standard methods described in ref. 8. The following antibodies required 40-minute citrate buffer antigen retrieval at 95°C: anti-phospho-ser139-γ-H2AFX (Cell Signaling Technology, clone 20E3, #9718), anti-vimentin (Cell Signaling Technology, clone D21H3, #5741). Anti-ATM antibody (0.12 mg/mL, Abcam, Y170, ab32420) was incubated overnight. For negative controls, the primary antibodies were omitted. The human stainings were evaluated by an experienced pathologist (B. Sipos). All patient data were blinded during the evaluation. ATM expression was graded as wild type (clear nuclear expression in >10% of the tumor cells) and as lost (no distinct nuclear stain in presence of internal positive controls, such as inflammatory cells of stromal cells). Weak to moderate ATM staining in <10% of the tumor cells was evaluated as low (indeterminate for ATM loss). Images were acquired on an Axioplan2 microscope (Carl Zeiss) equipped with an AxioCamHR camera and AxioVision Version 4.8 (both Carl Zeiss) software. Magnifications are provided in figure legends.

Immunofluorescence

Fifty percent to 60% confluent mouse PDAC cells were fixed with buffered paraformaldehyde 2% for 20 minutes at room temperature and permeabilized with Triton 0.7% for 15 minutes at room temperature. The fixed cells were incubated for 1 hour at room temperature with blocking solution (goat serum 5%, Triton 0.4%, BSA 1%) and then overnight at 4°C with primary antibodies: anti-phospho-ser10-H3 (1/250, Cell Signaling Technology, #9701), anti-phospho-ser824-KAP1 (1/500, Bethyl Laboratories, A300-767A), anti-phospho-ser317 CHK1 (1/250, Bethyl

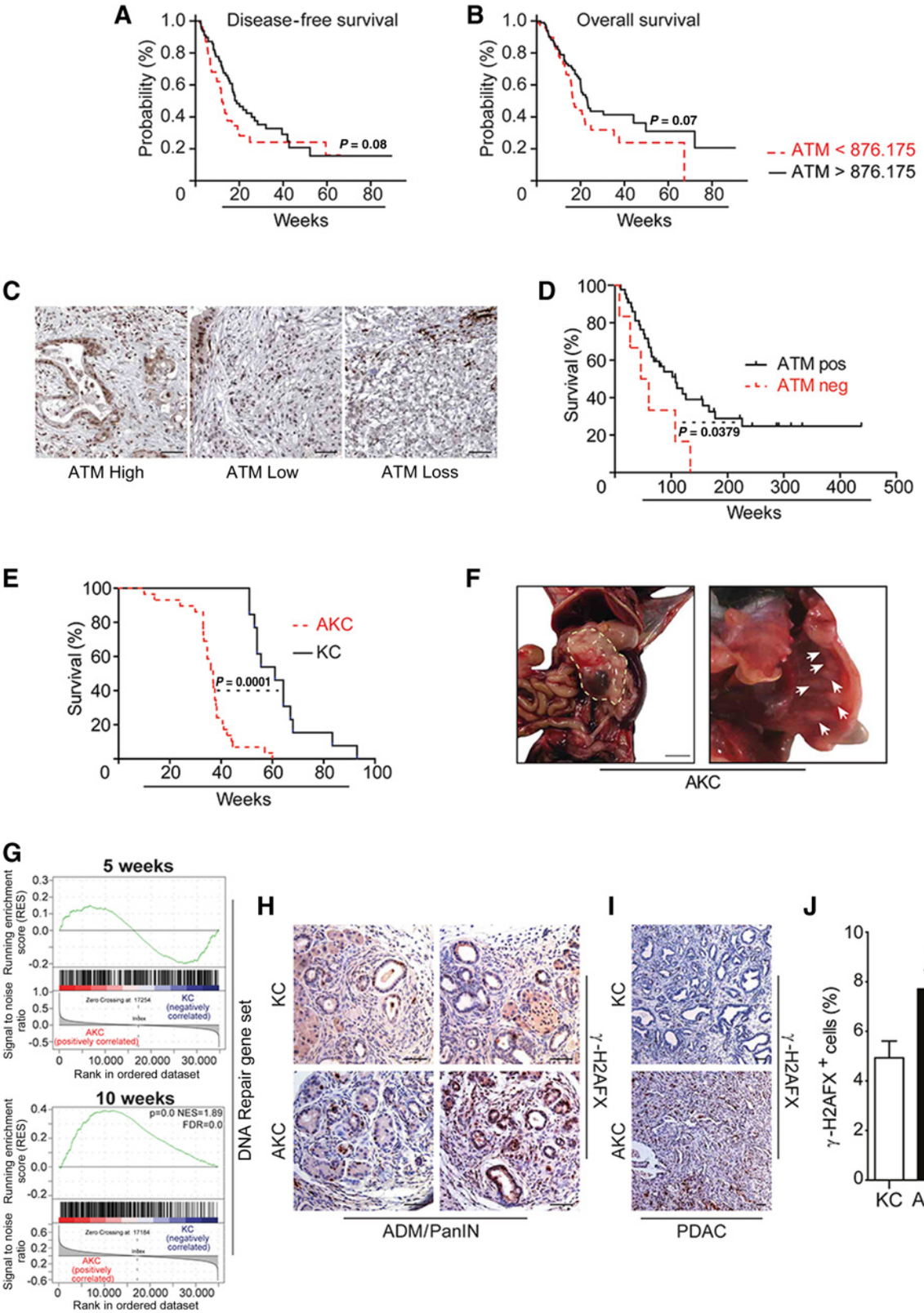

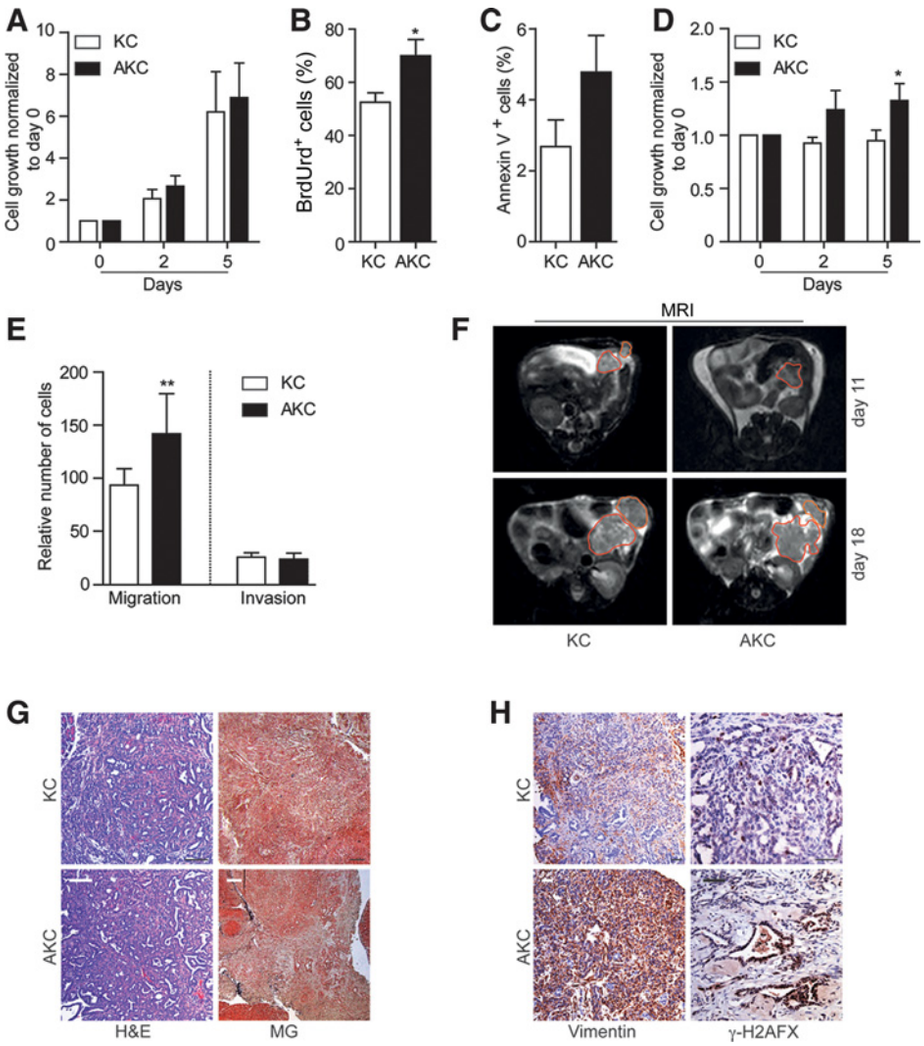

Figure 2.
ATM-depleted PDAC cell lines mimic the AKC mice phenotype. **A,** Cell growth assessment under normal culture conditions for KC versus AKC cell lines **B,** BrdUrd incorporation assay (*, $P = 0.0375$). **C,** Apoptosis analysis in KC and AKC lines. **D,** Growth curve under starvation conditions (*, $P < 0.05$). **E,** Quantitative assessment of migration and invasion assay (**, $P = 0.0011$). **F,** MRI confirmation of pancreatic tumor growth after injection of KC and AKC cell lines into SCID mice (outlined in red). **G,** IHC characterization of the orthotopic transplanted tumors with hematoxylin and eosin (H&E), Masson–Goldner (MG; scale bar, 20 μm), **H,** Vimentin and γ-H2AFX stainings. If not stated otherwise, scale bars are 100 μm.

Laboratories, A300-163A), anti-TRP53 CM5 (1/500, Novocastra, NCL-p53-CM5p), anti-ser139-γ-H2AFX (1/500, Millipore, JBW301), and anti-53BP1 (Novus Biological, NB 100-304).

Inhibitors

Gemcitabine (Fresenius Kabi Deutschland GmbH, L01BC05 and Hexal AG), olaparib (Hycultec GmbH, HY-10162-100 and Axon Medchem, AZD2281), 5-fluorouracil (5-FU; Sigma-Aldrich F6627), ATR inhibitor VE-822 (ATRi, Abmole, M3115), niraparib (Selleckchem S7625). If not stated, the used concentrations for *in vitro* studies were gemcitabine 10 ng/mL, olaparib 5 μmol/L, 5-FU 200 μg/mL, and ATRi 0.1 μmol/L. For *in vivo* studies, gemcitabine (Hexal) was administered on day 10, 17, and 24, intraperitoneally at a concentration of 100 mg/kg. Olaparib (Axon Medchem, AZD2281) was dissolved in DMSO to a final concentration of 50 mg/mL and then added to 10% 2-hydroxy-propyl-beta-cyclo-dextrin/PBS solution. Olaparib was administered daily for 14 days at a dose of 50 mg/kg i.p. The ATR inhibitor VE-822 (Abmole, M3115) was dissolved in an equilibrated (v/v) mixture PBS (70%), polyethylene glycol 300 (PEG300, 29.5%), and Tween 80 (0.5%) at a concentration of 18 mg/mL. VE-822 was administered on days 10 to 13 and 17 to 20 at a dose of 30 mg/kg by oral gavage.

Figure 1.
Low ATM expression in PDAC shortens survival in mouse and human. **A,** Disease-free survival in PDAC patients related to *ATM* mRNA expression levels (cutoff 876.125, $P = 0.08$). **B,** Overall survival depending on ATM expression levels in PDAC patients (cutoff 876.125, $P = 0.07$). **C,** Representative IHC images of human PDAC TMA with various expression levels of ATM (scale bar, 20 μm). **D** and **E** Kaplan–Meier analysis of overall survival of 49 patients related to ATM expression ($P = 0.0379$; **D**) and of overall survival in KC ($n = 13$) and AKC ($n = 29$) mice ($P = 0.0001$; **E**). **F,** Representative macroscopic images of an AKC mouse situs and diaphragm metastasis. **G,** GSEA of a DNA repair gene set in 5 and 10-week-old murine pancreata. **H,** Representative γ-H2AFX immunostaining in ADM and PanIN lesions of KC and AKC mice (scale bar, 20 μm). **I,** Overview of γ-H2AFX staining in KC and AKC-derived PDAC (scale bar, 20 μm). **J,** Quantitative analysis of γ-H2AFX in dysplastic lesions of 10-week-old mice (*, $P = 0.0169$).

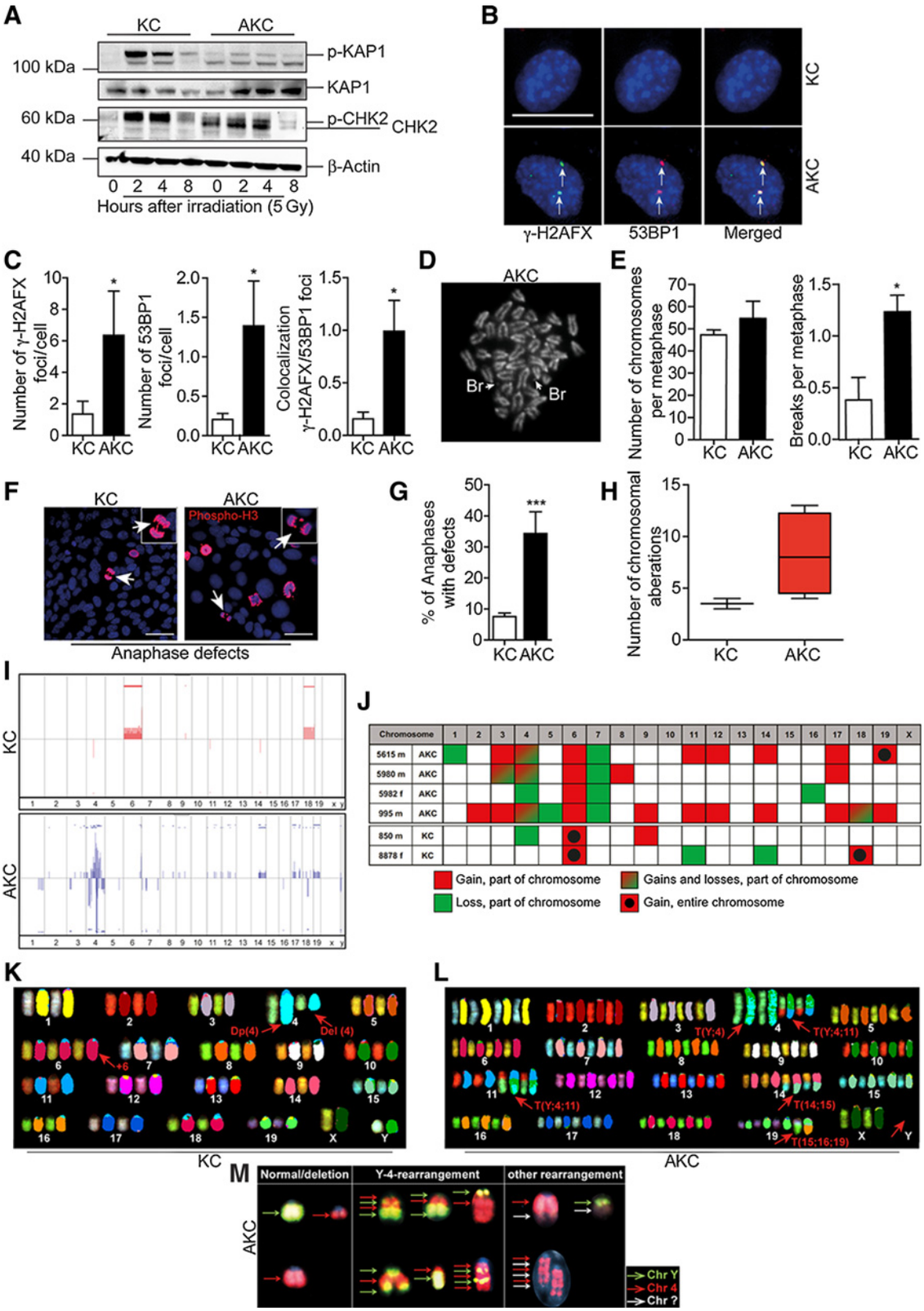

Western blot analysis

The cells were harvested 2, 4, and 8 hours upon 5 Gy IR. Cells were lysed in ice-cold protein lysis buffer (HEPES 20 mmol/L, glycerol 20%, NaCl 500 mmol/L, $MgCl_2$ 1.5 mmol/L, EDTA 0.2 mmol/L, DTT 1 mmol/L, NP-40 1%) containing a protease inhibitor cocktail (cOmplete mini EDTA-Free, Roche) for 30 minutes at 4°C. Lysates were then sonicated for 10 seconds. The Western blot analysis was performed using NuPAGE Novex 4% to 12% Bis-Tris Protein gels (Invitrogen) and NuPAGE MOPs SDS Running Buffer (Invitrogen), blotted into a nitrocellulose membrane (Hybond ECL, Amersham Biosciences) and finally developed using the ECL Prime Chemiluminescence Kit (Amersham Biosciences). The following antibodies were used: anti-phospho-ser824-KAP1 (1/1000, Bethyl Laboratories, A300-767A), anti-KAP1 (1/1000, Bethyl Laboratories, A300-274A), anti-CHK2 (BD biosciences, 611570), anti-β-actin (Cell Signaling Technology, #4970).

Colony formation assay

A total of 1,000 cells were seeded in 6-well plate or 12-well plate and incubated with olaparib (5 μmol/L), gemcitabine (10 ng/mL), and ATR inhibitor VE-822 (0.1 μmol/L) for 72 hours or irradiated with 5 or 10 Gy. Fourteen days after the beginning of the treatment, the colonies were fixed with methanol, stained with GIEMSA, and counted.

Gene expression microarrays

Gene expression microarrays were performed as described in ref. 5. The gene set used for the DNA repair gene set enrichment analysis (GSEA) is provided in Supplementary Table S1. Array data are available in GEO under accession code GSE68808.

Metaphase preparation

The preparation of the cells was done as described in ref. 9. For each cell line, 40 metaphases were evaluated regarding chromosome number, break, and fusion.

Cell viability assay

Cell viability measurement was performed using a MTT assay according to the manufacturer's recommendations (Sigma-Aldrich, M2128).

aCGH

aCGH was performed using a SurePrint G3 mouse genome CGH Microarray Kit (4 × 180K, Design ID 027411; Agilent Technologies). As reference DNA, we used pooled DNA from male or female mice from the same mouse strain. Samples were labeled with the Agilent SureTag DNA Labeling Kit (Agilent Technologies) according to the manufacturer's instructions. Slides were scanned using an Agilent microarray scanner G2505B, and data were analyzed using Genomic Workbench 7.0 (both from Agilent Technologies) with the statistical algorithm ADM-2.

Spectral karyotyping

Spectral karyotyping (SKY) was performed using the ASI SkyPaint DNA Kit M-10 for mouse chromosomes as described before (10, 11). Ten cells per cell line were analyzed. In addition, selected whole chromosome painting was carried out on AKC and KC cells.

DNA fiber spreading assay

The DNA fiber assay was performed as described in ref. 12.

Statistical analysis

All experiments were repeated independently at least 3 times, and error bars in the graphs show the calculated standard error of the mean. Statistical significance was calculated using an unpaired Student t test, Mann–Whitney test or one-way ANOVA unless otherwise stated. Kaplan–Meier curves were calculated using the survival time for each mouse from all littermate groups. Human data were obtained from a characterized PDAC cohort of Goettingen University (Goettingen, Germany; $n = 80$). Patients were selected for full availability of datasets: date of primary diagnosis, date of death or last contact, confirmed PDAC histology, lymph node status, and resection margins, resulting in 49 patients meeting the criteria. Survival times below 50 days postoperative were excluded to prevent a non–disease-related bias ($n = 2$). Kaplan–Meier curves were calculated from primary diagnosis of PDAC until death or last patient contact (censored). The log-rank (Mantel–Cox) test was used to test for significant differences between the groups. Statistically significant differences were considered by the P values <0.05. GraphPad Prism 7 was used for statistical analysis and graphical presentation.

Results

AKC mice recapitulate human PDAC biology

To corroborate our previous findings in human PDAC (8), we exploited complete datasets available at www.cbioportal.org. Here, defined mRNA thresholds separated two patient groups with a shorter progression-free and overall survival in the ATM low groups ($P = 0.07$ and $P = 0.08$ for PFS and OS; Fig. 1A and B). Next, an independent cohort of resected human PDAC was analyzed via immunostaining for ATM (13). Interestingly, we observed areas of clonal ATM loss along with a weak staining pattern, leading to a correlation between ATM protein expression

Figure 3.

ATM deficiency causes impaired DDR and promotes genomic instability. **A,** Western blot confirmation of common ATM DDR targets in KC and AKC cells after 5 Gy γ-irradiation. **B,** Representative pictures of γ-H2AFX and 53BP1 immunofluorescence staining (scale bar, 20 μm). **C,** Quantitative analysis of immunofluorescence stainings for γ-H2AFX (*, $P = 0.0289$), 53BP1 (*, $P = 0.0286$)-positive foci, and colocalization (*, $P = 0.0286$). **D,** Illustration of a metaphase with emphasized chromosomal breaks (arrows) in an AKC cell line (magnification, ×600). **E,** Quantitative analysis of metaphases revealed aneuploidy in KC and AKC cell lines. ATM deficiency is associated with increased chromosomal breaks (*, $P = 0.0331$). **F,** Representative images of phospho-ser10-H3 immunofluorescence staining showing typical anaphase anomalies (arrows). Scale bar, 20 μm; insets magnification, ×600. **G,** Percentage of defective anaphases in KC and AKC cell lines (***, $P = 0.0004$). **H,** Number of chromosomal aberrations with array CGH of KC and AKC cell lines. **I,** Overview of array CGH of KC and AKC cell lines. AKC cell lines show recurrent chromosome 4 aberrations. **J,** Detailed chromosomal alterations in 2 KC and 4 AKC cell lines. **K** and **L,** Representative SKY analysis of a KC (**K**) and an AKC (**L**) cell line with the recurrent translocation T(4, Y). **M,** Illustration of chromothripsis involving chromosome 4 and Y in AKC cell lines.

and survival in a cohort of 49 resected human PDACs (Fig. 1C and D).

To explore the consequences of ATM deficiency on pancreatic cancer development and progression, we utilized KC mice that had been crossed with conditional $Atm^{floxed/floxed}$ mice to generate animals with pancreas-specific deletion of *Atm* (AKC; ref. 5). Extended breeding of these mice confirms our previous data showing a significantly reduced survival of ATM-deficient mice (AKC), with a median survival of 36.9 weeks for homozygous ($n = 29$) *Atm*-targeted animals, compared with 61 weeks for KC mice ($n = 13$) in a Kaplan–Meier survival analysis (hazard ratio, 0.281; Fig. 1E). AKC mice developed large PDACs with a strong invasive potential, leading to a high frequency (50%) of lung, peritoneal, or hepatic metastases (Fig. 1F; ref. 8).

Substantial DNA damage during pancreatic cancer formation

ATM is one of the key components of the DNA repair machinery. Furthermore, ATM is recurrently inactivated by various mutational mechanisms in human PDAC (14). We employed previously generated comparative genome-wide transcriptional profiling sets and analyzed these data by GSEA from age-matched (5 and 10 weeks) KC and AKC mice (8) and plotted a predefined gene set implicated in "DNA repair" (Supplementary Table S1; Fig. 1G). Although there was no enrichment in 5-week-old pancreata lacking gross dysplasia, GSEA was highly significant in 10-week-old AKC mice pointing toward a causal link between the observed dysplasia and disturbed genome integrity (Fig. 1G). Similar enrichment was found in ATM-deficient samples from a mouse model resembling chronic lymphatic leukemia (Supplementary Fig. S1).

A key response to DNA DSBs is the formation of nuclear foci, which contain phosphorylated histone H2AFX (γ-H2AFX; refs. 15–17). γ-H2AFX foci were found in both ADM and PanIN lesions in AKC and KC mice. Overall, the total amount of γ-H2AFX–positive cells within dysplastic lesions was higher in AKC mice (Fig. 1H). A similar phenotype was observed in AKC-derived PDACs (Fig. 1H–J). In conclusion, there is substantial DNA damage in both genotypes (18), while *Atm* deletion leads to an overall increase of damage carrying dysplastic and also cancerous cells.

ATM-deficient PDAC lines mimic phenotypes observed in AKC mice

We isolated tumor cells and generated stable cell lines from AKC and KC tumors. Overall, growth behavior was similar in both genotypes but the number of BrdUrd-incorporating cells was slightly higher on expense of a trend toward more apoptotic cells in AKC lines (Fig. 2A–C). Stress conditions mimicked by serum starvation clearly revealed a higher proliferative capacity in AKC cell lines (Fig. 2D). Migratory properties were also higher in AKC, while invasion remained unchanged in both genotypes (Fig. 2E). To further proof the value of these cell lines as an *in vitro* tool, we conducted orthotopic transplantation into the pancreas. Rapid PDAC formation and vast metastatic disease were observed leading to accelerated signs of wasting in both genotypes. Spontaneous tumor growth kinetics were similar as shown by timed MRI (Fig. 2F). Hematoxylin/eosin and Masson–Goldner stainings confirmed the previously reported stroma-rich pancreatic cancer phenotype caused by ATM depletion (Fig. 2G). AKC tumors also contained more cells staining positive for vimentin, underpinning our previous observations of an EMT-rich cancer upon *Atm* deletion (Fig. 2H; ref. 8). Finally, the arising cancers from AKC lines showed increased γ-H2AFX foci (Fig. 2H).

ATM preserves genome integrity, and its deficiency leads to chromosomal instability

It has previously been shown that primary ATM-deficient cells exhibit an altered DDR upon ionizing radiation (IR; ref. 14). To analyze whether AKC cell lines exhibit similar defects, we monitored DDR activity upon 5 Gy of IR. As expected, KC cell lines exhibited ATM-mediated phosphorylation marks on known ATM substrates, such as KAP1 and CHK2 (Fig. 3A). In sharp contrast, AKC cell lines showed a complete lack or severely reduced phosphorylation of these proteins, indicating a substantially impaired DDR (Fig. 3A).

53BP1, as well as γ-H2AFX are detectable in nuclear foci after DNA damage, such as DSBs or replicative stress (12, 17). In line with our observation in tissue, AKC cells showed a significant, 4-fold increase of γ-H2AFX foci accumulation, compared with KC cells (Fig. 3B and C). 53BP1 foci numbers were even 7-fold elevated in AKC, compared with KC (Fig. 3B and C). To investigate whether γ-H2AFX foci label indeed for DSBs rather than for alternative DNA lesions, such as sites of replication stress, we compared 53BP1 foci colocalization in the two cell genotypes. Correspondingly, the number of γ-H2AFX and 53BP1 double-positive foci showed a 6-fold increase in ATM-deficient cells (Fig. 3B and C).

It remains largely unclear to what extent these DSBs cause genomic instability. Therefore, we performed metaphase analysis on AKC and KC lines, which both exhibit aneuploidy (Fig. 3D and E). Nevertheless, there were significantly more chromosomal breaks in the AKC genotype (Fig. 3E). Consistently, we found significantly more anaphase defects in ATM-deficient PDAC lines, compared with ATM-proficient KC cells (Fig. 3F and G). aCGH analysis found the frequency of chromosomal aberrations significantly higher with 8.25 versus 3.5 aberrant chromosomes in AKC versus KC cell lines (Fig. 3H). Intriguingly, certain aberration hotspots, such as chromosome 4, were specifically observed in ATM-deficient PDAC cell lines (Fig. 3I and J).

Complex structural aberrations including chromothripsis in AKC lines

SKY confirmed significantly more chromosomal instability in AKC cells compared with KC cells (Fig. 3K and L; Supplementary Table S2). Up to two simple structural aberrations and one to four numerical aberrations per cell were identified in controls (Fig. 3K; Supplementary Table S2). In AKC cell lines, up to 7 structural anomalies, including several complex aberrations, were evident from SKY in nearly all cells (Fig. 3L). Furthermore, up to 17 additional aberrations were found only once in AKC cells, but not in KC cells. In line with the aCGH data, chromosome (Chr) 4 was affected most often by structural rearrangements. In addition, several structural rearrangements affecting Chr Y were observed in male cell lines (Fig. 3L). Several cells also showed loss of Chr Y in DAPI display. However, fluorescent signals from SKY showed overlaps of spectra marking Chr Y and Chr 4 in these cells (Fig. 3L), indicating possible chromothripsis of Chr 4 and Chr Y in AKC cells and incorporation of the shredded Chr Y in other chromosomes, preferentially 4. Whole chromosome paint of Chr Y and 4

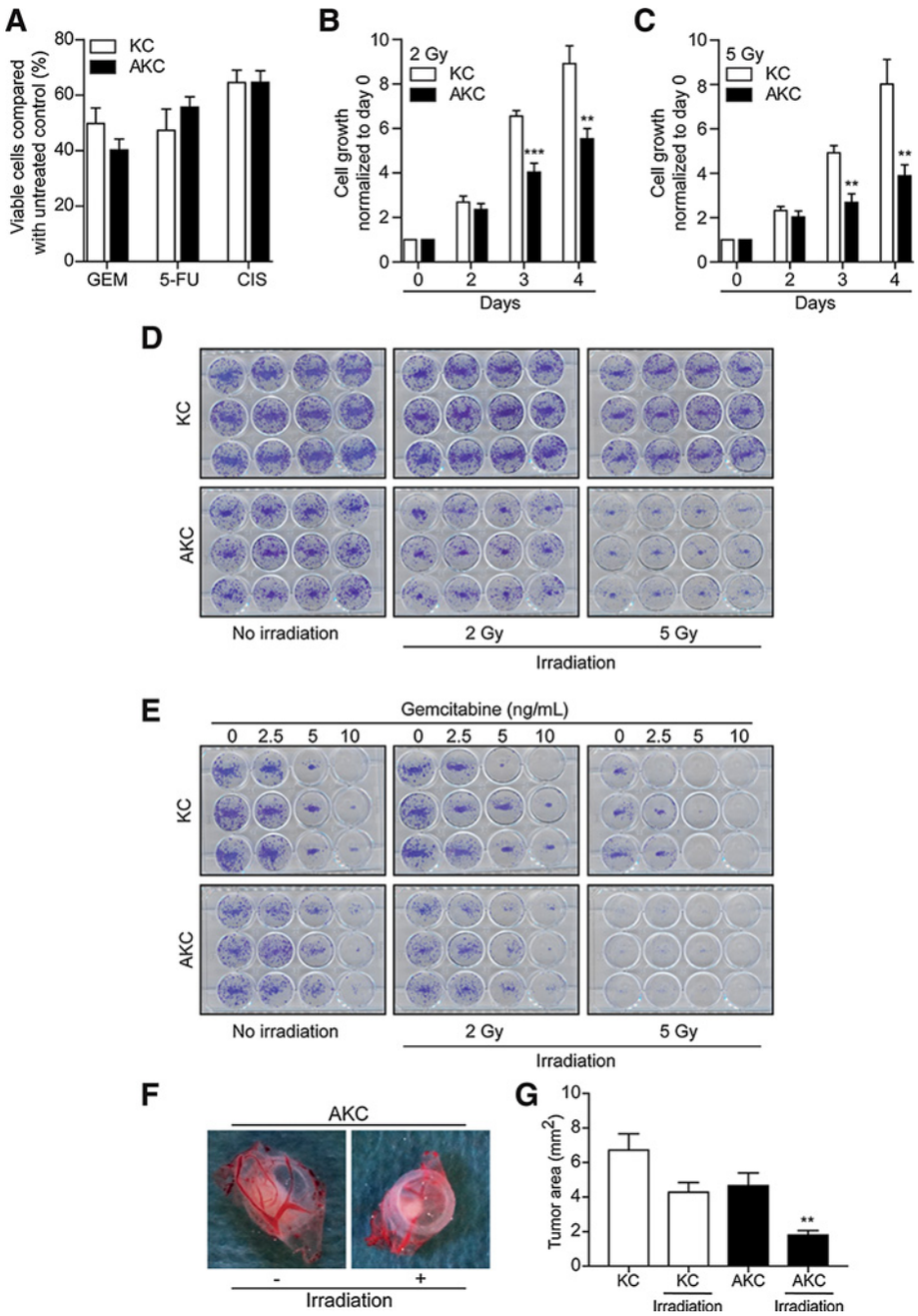

Figure 4.

ATM deficiency sensitizes PDAC against irradiation. **A,** Cell line sensitivity analyzed by MTT assay to gemcitabine (GEM), 5-FU, and cisplatin (CIS). **B,** AKC cell lines exhibit sensitivity to IR after 3 (***, $P = 0.0007$) and 4 days (**, $P = 0.0041$) upon 2 Gy (**, $P = 0.0039$; **B**) and 5 Gy (**, $P = 0.0050$; **C**). **D** and **E,** Colony formation assay of KC and AKC cell lines in response to single-dose IR (**D**) and to gemcitabine + IR (**E**). **F,** AKC-derived CAM-based tumor formation ± IR (5 Gy). **G,** Quantitative tumor volume assessment of KC and AKC-derived CAM tumors ± IR (5 Gy; **, $P = 0.0011$).

confirmed several complex structural rearrangements of these two chromosomes and further substantiated possible chromothripsis (Fig. 3M).

DDR defects sensitize ATM-deficient PDAC toward additional genotoxic stress

Next, we applied the DNA crosslinking agent cisplatin, the antimetabolite fluoropyrimidine 5-FU and the cytotoxic cytidine analogue gemcitabine to both genotypes without observing any differences in growth kinetics as assessed by MTT assays (Fig. 4A). Gemcitabine had the strongest impact on tumor cell viability and colony formation in both genotypes (Fig. 4A). A series of clinical trials have failed to demonstrate a substantial benefit of γ-irradiation on PDAC (19). However, neither of these studies took gene mutations within the DDR machinery into account, which were shown to establish a genomic unstable subtype of human PDAC (8). The growth of KC lines remained unaltered upon different doses of γ-irradiation while AKC counterparts displayed significantly perturbed growth (Fig. 4B and C). Clonogenic colony survival assays corroborated these findings (Fig. 4D and E). Additive treatment with gemcitabine and γ-irradiation further potentiated this effect (Fig. 4E). Having determined the effect of γ-irradiation *in vitro*, we further evaluated tumor-forming capacity *in vivo*, using the chicken chorioallantoic membrane (CAM)

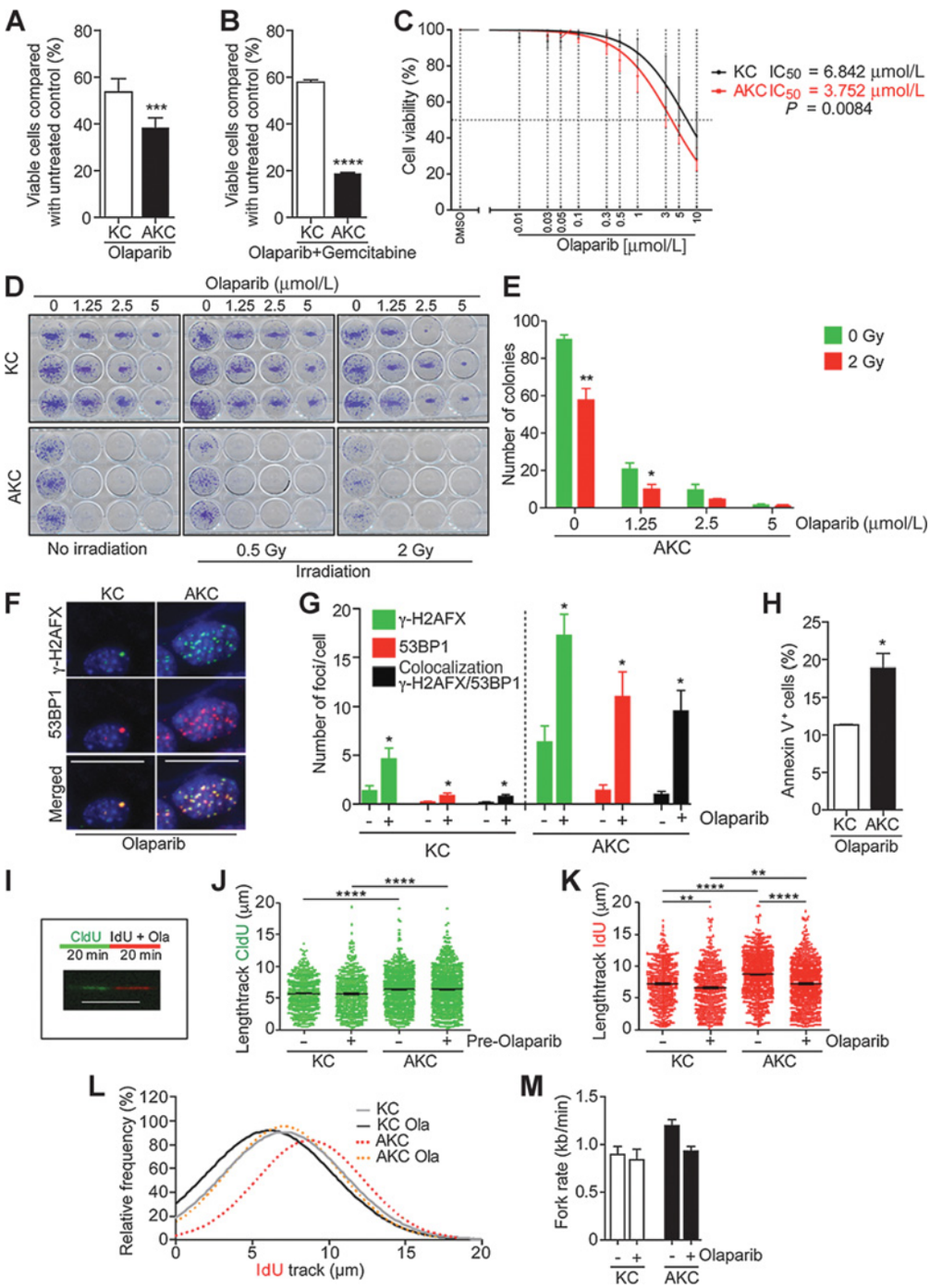

Figure 5.

ATM deficiency sensitizes PDAC cell lines to PARP inhibition. **A,** MTT assay analysis of olaparib (5 µmol/L; ***, $P < 0.001$; **B**) plus gemcitabine (5 ng/mL; ****, $P < 0.0001$)–treated KC and AKC cell lines. **C,** Olaparib IC_{50} curve in KC versus AKC cell lines ($P = 0.0084$). **D,** Colony formation assay of KC and AKC cells lines upon olaparib ± irradiation. **E,** Quantitative analysis of the colony formation assay. **F,** Immunofluorescence staining of γ-H2AFX and 53BP1 foci and their colocalization. **G,** Increased number of γ-H2AFX (*, $P = 0.0286$), 53BP1 (*, $P = 0.0286$)–positive foci, and colocalization (*, $P = 0.0286$) ± olaparib treatment (5 µmol/L) in AKC versus KC cells. **H,** Apoptosis measurement upon olaparib treatment. **I,** DNA fiber-spreading assay in KC and AKC cells ± olaparib treatment. Schematic technical overview and representative fiber image (scale bar, 10 µm; **, $P < 0.01$; ****, $P = 0.0001$). *P* values were calculated by two-tailed Mann–Whitney test. **J–L,** Nascent DNA replication track length is displayed as distribution of relative track length frequency, whereby the maximum value of the bin center of each dataset was defined as 100%. **M,** Graphic presentation of mean values of fork rates and SEM calculated from total IdU track lengths ± olaparib treatment from two independent experiments.

model. Also in this assay, pretreatment with 5 Gy γ-irradiation revealed a significant effect ($P = 0.0011$) on tumor growth in AKC compared with KC lines (Fig. 4F and G).

Synthetic lethality between *Atm* deletion and PARP inhibition in PDAC

Two major DSB repair pathways, namely nonhomologous end joining (NHEJ) and homologous recombination (HR), are employed by mammalian cells, the latter being strongly dependent on ATM (14). PARP1 plays a critical role in base excision repair and PARP1 deficiency usually causes stall of the replication fork during DNA replication and subsequent accumulation of DSBs (20). Moreover, PARP1 is crucially involved in alternative end joining (21). Synthetic lethality has been observed upon BRCA1/2 loss and PARP1 inhibition in several cancers (22). As ATM loss can limit HR activity (23), PARP1 might also be a druggable target in ATM-deficient PDAC. Olaparib robustly diminished cell viability and induced cell death in an ATM-dependent manner (Fig. 5A). This effect was substantially potentiated by combining olaparib with gemcitabine (Fig. 5B). IC_{50} values significantly differed in both genotypes (KC $IC_{50} = 6.842$ μmol/L; AKC $IC_{50} = 3.752$ μmol/L; $P = 0.0084$) (Fig. 5C). Similar discrimination could be observed with another PARP inhibitor niraparib (KC 51.6 μmol/L; AKC 8.664 μmol/L; $P < 0.0001$). To corroborate these data, clonogenic survival assays were performed. Synthetic lethality of ATM deficiency and PARP inhibition was even more pronounced, leading to a remarkable and dose-dependent decrease in colony formation (Fig. 5D). To elucidate possible potentiating effects with other therapies, γ-irradiation was used together with reduced dosages of olaparib. The combined treatment allowed dose saving of olaparib in the context of low-dose γ-irradiation with similarly ablated colony formation in AKC cells (Fig. 5D and E).

Atm deletion and PARP1 inhibition synergistically cause accumulation of DSBs in PDAC

To investigate whether the increased PARP inhibitor sensitivity of ATM-deficient cells is caused by impaired DNA repair, γ-H2AFX and 53BP1 foci accumulation was examined (Fig. 5F and G). Olaparib treatment led to a 3-fold increase in γ-H2AFX (1.35 vs. 4.62), a 4-fold increase in 53BP1 (0.20 vs. 0.87), and a 5-fold elevated number of colocalized foci (0.15 vs. 0.79) in KC cells. In AKC cells, PARP inhibition increased γ-H2AFX foci numbers again 3-fold (5.4 vs. 17.2); however, 53BP1 foci numbers and double-positive foci were elevated 8-fold (1.39 vs. 11.02) and 10-fold (0.99 vs. 9.5 foci), respectively. When we calculated the

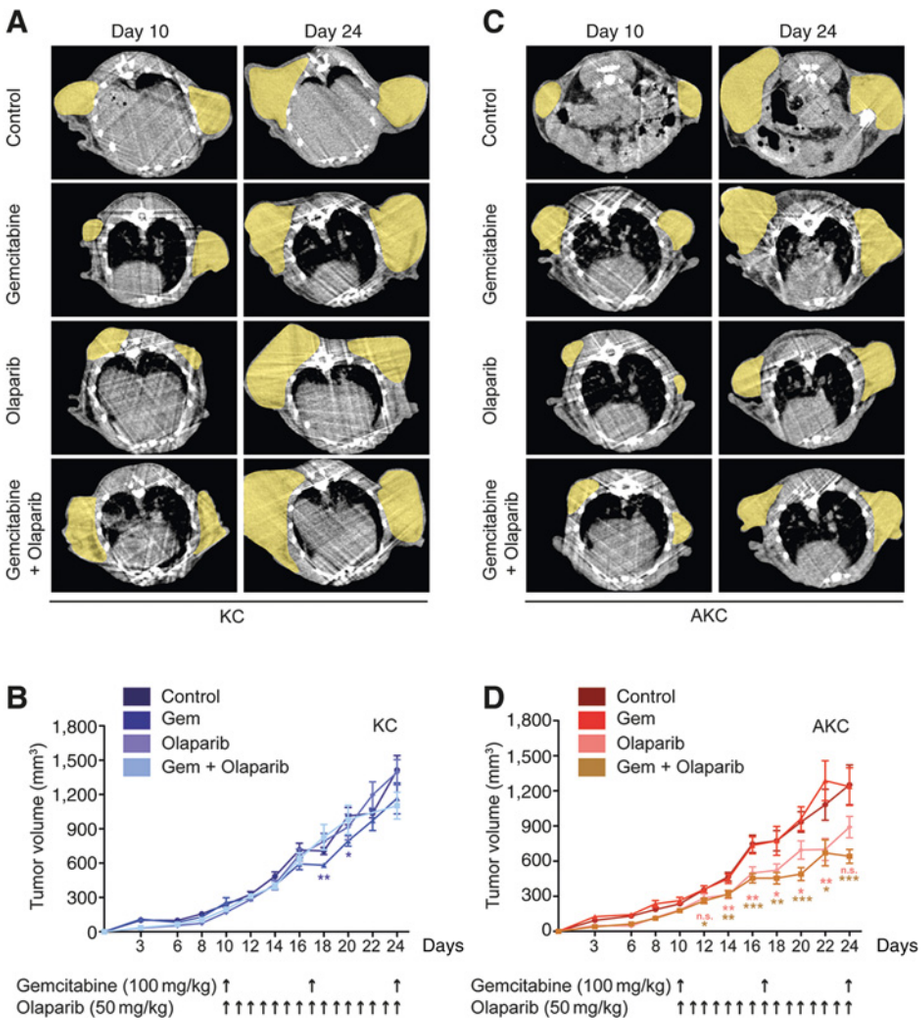

Figure 6.
ATM deficiency sensitizes to olaparib treatment *in vivo*. **A** and **C,** μCT-based response assessment of *in vivo* tumor formation of KC (**A**) and AKC (**C**) cell line. Mice were imaged before treatment start (day 10; left) and after 14 days on indicated treatments (day 24; right). Yellow areas, tumor lesions. **B** and **D,** Tumor volume was longitudinally measured for 24 days (*, $P < 0.05$; **, $P < 0.01$; ***, $P < 0.001$).

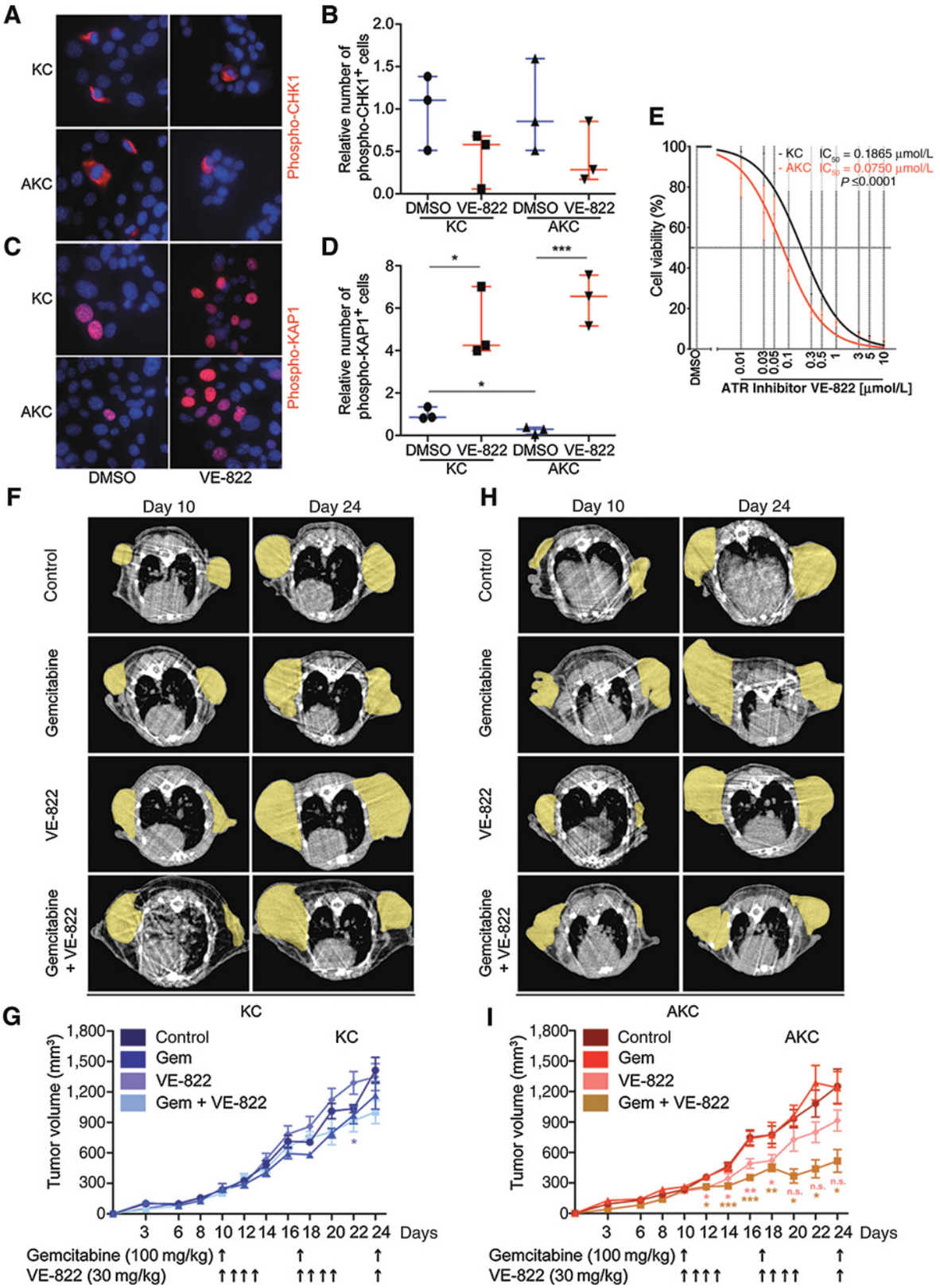

fraction of true DSBs arising upon treatment by comparing double-positive foci, we observed that 70% to 90% of the 53BP1 foci indeed colocalized with γ-H2AFX foci and therefore reflected DSBs in both genotypes (Figs. 3C and 5F and G). Remarkably, only 10% to 20% of γ-H2AFX foci in KC cells with or without olaparib and in untreated AKC cells colocalized with 53BP1 foci. For olaparib-treated AKC cells, this proportion drastically rose to >50% of the γ-H2AFX foci colocalizing with 53BP1. Taken together, ATM-deficient cells accumulate more DNA damage, in particular DSBs after olaparib treatment. Replication fork collapse due to DSBs in AKC lines may increase sensitivity to PARP inhibition, because PARP1 cannot longer reactivate forks and ATM deficiency compromises HR-mediated repair of collapsed forks (24). Consistent with this hypothesis, we observed a significant increase of apoptosis in AKC versus KC following olaparib treatment (Fig. 5H).

Replication elongation in ATM-deficient cells is diminished by PARP1 inhibition

AKC cells showed a dramatic accumulation of DSBs after replication stress–inducing treatment with the PARP inhibitor olaparib. To investigate whether *Atm* knockout affects DNA damage bypass following olaparib treatment, we performed DNA fiber assays (Fig. 5I–M). Interestingly, ATM deficiency led to a general statistically significant increase of the track lengths both during the 5-chloro-2-deoxyuridine (CldU) labeling period before treatment (Fig. 5J) as well as during 5-iodo-2-deoxyuridine (IdU) labeling in mock- and olaparib-treated cells (Fig. 5K). This suggested derepression of a DNA lesion bypass mechanism after *Atm* knockout. PARP inhibitor treatment itself caused a more pronounced track shortening in AKC cells, namely of 22% compared with 7% in KC cells. This track shortening becomes apparent also as a shift of the track length distribution curves (Fig. 5L). Moreover, we calculated replication fork rate decreases from 0.92 to 0.86 kb*min^{-1} in KC and from 1.14 to 0.93 kb*min^{-1} in AKC cells after PARP inhibition (Fig. 5M). From this, we conclude that AKC cells exhibit an accelerated basal progression of the replication fork compared with KC cells. Accelerated replication could be explained by alternative bypass mechanisms involving translesion synthesis or fork regression, the latter of which is blocked by PARP inhibitors (24).

Selective single-agent efficacy of olaparib on ATM-deficient KRAS-driven PDAC *in vivo*

To finally validate our *in vitro* observations, we transferred our findings to an *in vivo* model. Here, we assessed the therapeutic efficacy of olaparib alone and in combination with gemcitabine in a subcutaneous transplantation model of KC and AKC-derived tumors (Fig. 6A–D). Subcutaneous tumor growth was measured manually and complemented with μCT-morphologic tumor response data (Fig. 6A–D, Supplementary Figs. S2A–S2B and S3A–S3H). While KC tumors displayed continued tumor growth under olaparib treatment, AKC tumors remained largely stable in size (Fig. 6A–D; Supplementary Figs. S2A–S2B and S3A–S3H). This led to significantly smaller AKC tumors in response to olaparib compared with KC counterparts (Supplementary Fig. S3A–S3H). We note that vehicle-treated KC and AKC-derived tumors displayed continuous growth throughout the entire observation period of 21 days (Fig. 6B and D). Interestingly, the combination therapy with gemcitabine and olaparib revealed the expected benefit as suggested from our *in vitro* data and was most efficient in tumor growth stabilization (Fig. 6D; Supplementary Fig. S2A and S2B).

ATM deficiency sensitizes PDAC cell lines to ATR inhibition

Next, we performed semiquantitative immunofluorescence analysis for a set of ATM-downstream targets within the DDR, (i) phospho-ser824-KAP1, a common target of ATM/PRKDC (DNA-dependent protein kinase; ref. 25) and (ii) phospho-ser317-CHK1, a specific target of ATM/ATR. Here, both KC and AKC cells exhibited CHK1 and KAP1 phosphorylation at basal levels. Interestingly, while the phospho-CHK1 levels were only slightly lower in AKC lines, basal KAP1 phosphorylation was significantly lower in ATM-deficient lines (Fig. 7A and B). Next, replicative stress was mimicked by ATR inhibition, followed by counting phospho-ser824-KAP1 and phospho-ser317-CHK1–positive cells. Interestingly, the reduction of p-CHK1–positive cells upon ATR inhibition occurred independent of the ATM genotype but again appeared slightly but nonsignificantly lower in AKC lines (Fig. 7A and B). Vice versa, we measured a tremendous increase of phospho-ser824-KAP1 staining in both genotypes upon ATR inhibition (Fig. 7C and D). Intriguingly, the fold induction was much higher in the AKC genotype (5.5-fold KC vs. 43.9-fold AKC). KAP1 is phosphorylated by both ATM and PRKDC in a spatio-temporal manner (25) and the addiction of ATM-deficient tumors to PRKDC has been described previously (26). Taken together, by inhibiting alternate routes of ATM signaling in pancreatic cancer, it is suggested that ATR and to an even stronger extent PRKDC can compensate for ATM deficiency.

To corroborate these findings by functional assays, we inhibited ATR in KC and AKC cell lines. In line, the IC_{50} curve indicates a higher sensitivity of AKC cell lines toward ATR inhibition (Fig. 7E). We next assessed the therapeutic efficacy of an ATR inhibitor (VE-822) with or without gemcitabine in a subcutaneous transplantation model. Intriguingly, although ATR inhibition significantly reduced tumor progression from AKC lines, it had negligible effects on KC tumors (Fig. 7F and G; Supplementary Figs. S4A–S4B and S5A–S5H). The addition of gemcitabine relevantly strengthened the effects of ATR inhibition in AKC and was suitable to stabilize tumor growth (Fig. 7F–I; Supplementary Figs. S4A–S4B and S5A–S5H). Of note, VE-822 as a single agent was just capable to slow tumor growth

Figure 7.

ATM deficiency sensitizes to ATR inhibition *in vitro* and *in vivo*. **A** and **C,** Representative immunofluorescence images of phospho-CHK1 (**A**) and phospho-KAP1 (**C**) in KC and AKC cell lines ± VE-822 (magnification, ×600). **B** and **D,** Quantitative analysis of phospho-CHK1 (**B**) and phospho-KAP1–positive cells (**D**) ± VE-822 (1 μmol/L for 24 hours). ATR inhibition significantly increases phospho-KAP1–positive cells in KC ($P < 0.05$) and AKC cell lines ($P < 0.001$). **B** and **D,** Median box and whiskers plots for individual cell lines with minimum to maximum. Data were normalized to KC genotype under solvent (DMSO) conditions. Thereby, fold induction was calculated for phospho-KAP1 upon ATR inhibition, leading to a 5.5-fold increase in KC and a 43.9-fold increase in AKC lines. **E,** IC_{50} curve for the ATR inhibitor VE-822 with higher sensitivity of AKC cell lines ($P = <0.0001$). **F,** μCT-based response assessment of tumor formation revealed tumor growth in mice bearing KC-derived tumors independent of treatment regimen. **G** and **I,** Tumor volume was longitudinally measured for 24 days (*, $P < 0.05$; **, $P < 0.01$; ***, $P < 0.001$). **H,** μCT-based response assessment of AKC cell line–based tumor growth under indicated therapies. All mice were imaged before treatment start (day 10) and after 14 days on treatment (day 24). Yellow areas, tumor lesions.

at early time points in line with a stronger compensation by PRKDC in an ATM-deficient context.

Altogether, we show mechanistic differences between KC and AKC tumors and propose novel therapeutic approaches for ATM-deficient pancreatic cancer. Further research has to address compensating activity by other kinases in future studies.

Discussion

Individualized treatments for patients with metastatic PDAC have largely failed over the past decades. This is in part due to a lack of predictive biomarkers that take individual tumor characteristics into account (19). Next-generation sequencing efforts have indicated a broad genetic heterogeneity across several tumors but also within a given cancer (2, 27, 28). Thus, this vast load of intertumoral and intratumoral heterogeneity in PDAC makes it impossible to establish a universal treatment approach (2, 27, 28). Thus, defining individual subgroups is relevant from a pathophysiologic and oncological perspective to improve the outcome of PDAC treatment.

Genomic instability leading to, for example, aneuploidy, chromosomal aberrations, and copy number changes, has been considered as a hallmark of cancer, albeit it is not considered as the sole driving force to determine the degree of malignancy (29). Moreover, therapeutic inhibition of the DNA repair machinery helped to reach relevant improvements in subgroups of patients harboring particular mutations, such as BRCA1/2-mutated breast cancers (30). Whole-genome sequencing studies could also define subgroups of PDAC, including a genomically instable type (2). The latter was enriched for mutations of genes involved in regulating the DDR where ATM is one of the key players (14). Of note, oncogenic Ras signaling, the key driving module in PDAC, has been previously shown to limit the DDR and to stimulate base excision repair upon platinum-based treatment in lung cancer (31). These observations led us within this study to investigate the classical facet of ATM to preserve genome integrity upon repair of DNA DSBs (14). The altered DDR in *Atm* knockout PDAC led to a substantial increase in DSBs, in turn, leading to genomic instability with chromosomal gains and losses as well as dramatic translocations, including chromothripsis. Chromothripsis and polyploidization have been linked to an aggressive tumor behavior in multiple cancers, but not in PDAC (32). However, a recent study found in approximately two thirds of a large human PDAC cohort at least one chromothripsis event. This led to a dramatic loss of genetic information accompanied by the simultaneous knockout of several tumor suppressors (4). This scenario recapitulates the situation in PDAC patients with metastatic disease being frequently detectable already at diagnosis and high relapse rates upon curative resection far better than the "gradual accumulation of genetic burden" hypothesis (3, 4). This suggests that tumor evolution might be far more complex than expected, and more dramatic genetic events might pave the way for invasive growth. In line, novel preclinical model systems are warranted to reflect this genetically complex situation (4). Mice expressing pancreas-specific oncogenic KRAS together with knocked out *Atm* alleles might provide such a modeling tool.

Previously, we showed that Atm deletion drives EMT in PDAC (8). Quite recently, a zebra fish model for skin cancer exhibited genomic instability and EMT occurring together upon overexpression of CDC6 and C-MYC (33). In addition, TGFB1 induces EMT due to cytokinesis failure, which in turn leads to genomic instability specifically in cells that fail to undergo proliferation arrest (34). Thus, niche-derived extrinsic factors can trigger heritable structural genetic changes within cancer cells (34). These findings can be likely extrapolated to PDAC, a stroma-rich and genomically instable cancer known to cross-signal via TGFB1 with the stroma (35). Considering recent data putting the stroma in the center stage of PDAC treatment, inherited changes in the epithelial compartment driven by the stroma need to be kept in mind when developing novel treatments. Of note, *Atm* deletion establishes also a stroma-rich PDAC with hyperactive Nodal signaling (8).

Albeit DDR seems to be active in both genotypes, only AKC animals lack an appropriate DDR and develop signs of genomic instability. This is probably due to an attenuated capacity to repair DSBs upon *Atm* deletion opening a window of therapeutic intervention. On this note, base excision repair, nucleotide excision repair, NHEJ, and HR all involve PARP1, the most abundant member of the PARP enzyme family (36). The event catalyzed by PARPs is called PARylation and contributes to several aspects of DNA repair (36–38). In turn, PARP1 inhibition might offer a personalized medicine approach for ATM low PDAC. Of note, *BRCA1/2*-mutated PDAC has shown favorable results, building the basis for a currently recruiting phase III trial for this PDAC subset (https://clinicaltrials.gov/ct2/show/NCT02184195). Various other types of tumors, including breast cancer with *BRCA1/2*, have shown beneficial results (36). Synthetic lethality between PARP1 inhibition and depletion of various other DDR proteins suggested a "BRCANess signature" in cancers, which determines therapeutic response and may be actionable in a larger subgroup of tumors (2, 36). To this point, preclinical studies using olaparib in ATM-deficient chronic lymphoblastic leukemia cells also showed promising results in slowing down tumor progression and hypersensitivity to PARP inhibition (26, 39, 40). It is proposed that olaparib promotes PARP trapping on DNA, triggering replication fork collapse and cell death. This process is more pronounced in highly dividing cells (20). However, the only minor difference in the proliferative capacity in AKC tumor cell lines is unlikely to account for the dramatic response observed in our preclinical *in vivo* model. Similarly, a study in ATM-null, KRAS-driven lung cancer also observed pronounced efficiency of olaparib in combination with topoisomerase inhibitors (41). Clinical trials are urgently warranted to extend PARP1 inhibiting regimens to ATM low PDAC that constitute a substantial subgroup of about 10% of PDAC patients (8). The high rate of DSBs and the suggested sensitivity toward γ-irradiation might provide additional benefits and eventually start a good rationale for radiotherapy in PDAC. Despite these promising data, the PDACs were not entirely devitalized by PARP1 inhibition but instead continued to grow at a slower pace, suggesting a certain degree of intrinsic or acquired resistance (42, 43). It will be interesting to determine whether and which mechanism(s) apply for resistance in PDAC and to what extent can medical treatment circumvent this phenomenon (44). In our model, we noted putative compensation by alternate signaling routes bypassing ATM. Based on analyzing downstream targets, the strongest compensating kinase appears to be PRKDC and to a lower extent ATR. Consistent with this finding, addiction of ATM-deficient tumors to PRKDC has been described previously (26), and PRKDC was shown to partially substitute to ATR in replicative stress response (45) and to also phosphorylate KAP1 in absence of ATM (25). This compensation might establish another putative synthetically lethal therapeutic option for ATM-null PDAC. Nevertheless, ATR inhibition

was efficient in ATM-null PDAC cells *in vitro* and at least partially *in vivo* and could be boosted by a combination with gemcitabine. It is likely that the ablation of any remaining DNA repair capacity in ATM-null cells leads to synthetic lethality by a nontolerated mitotic catastrophe (46).

Taken together, our work provides several lines of novelty: (i) an intimate link between stromal content, genomic instability, and EMT (8); (ii) a preclinical model with virtually all hallmarks of human PDAC, including chromothripsis; (iii) a mechanistic work up explaining how *Atm* deletion leads to genomic instability; and (iv) two synthetic lethality pathways to allow precision medicine in ATM low patients. This paves the way for bench-to-bedside applications in an accelerated manner to test already available and approved drugs in the context of a relevant PDAC subset, the up to 10% of *ATM*-mutated human patients.

Disclosure of Potential Conflicts of Interest

E. Schröck is a consultant/advisory board member for ASI Advisory Board. No potential conflicts of interest were disclosed by the other authors.

Authors' Contributions

Conception and design: L. Perkhofer, M. Wagner, L. Wiesmüller, H.C. Reinhardt, P.-O. Frappart, A. Kleger

Development of methodology: L. Perkhofer, M.C.R. Carrasco, R. Russell, M. Wagner, H.C. Reinhardt, P.-O. Frappart, A. Kleger

Acquisition of data (provided animals, acquired and managed patients, provided facilities, etc.): L. Perkhofer, A. Schmitt, M. Ihle, S. Hampp, D.A. Ruess, E. Hessmann, R. Russell, A. Lechel, N. Azoitei, M. Lesina, H. Algül, E. Schröck, J. Gaedcke, M. Wagner, B. Sipos, P.-O. Frappart, A. Kleger

Analysis and interpretation of data (e.g., statistical analysis, biostatistics, computational analysis): L. Perkhofer, A. Schmitt, M.C.R. Carrasco, M. Ihle, S. Hampp, D.A. Ruess, E. Hessmann, R. Russell, A. Lechel, N. Azoitei, Q. Lin, S. Liebau, M. Hohwieler, H. Bohnenberger, M. Lesina, H. Algül, L. Gieldon, E. Schröck, J. Gaedcke, M. Wagner, L. Wiesmüller, B. Sipos, T. Seufferlein, H.C. Reinhardt, P.-O. Frappart, A. Kleger

Writing, review, and/or revision of the manuscript: L. Perkhofer, A. Schmitt, M. Ihle, S. Hampp, D.A. Ruess, A. Lechel, N. Azoitei, Q. Lin, S. Liebau, H. Algül, L. Gieldon, E. Schröck, L. Wiesmüller, B. Sipos, H.C. Reinhardt, P.-O. Frappart, A. Kleger

Administrative, technical, or material support (i.e., reporting or organizing data, constructing databases): H. Bohnenberger, T. Seufferlein, H.C. Reinhardt, P.-O. Frappart, A. Kleger

Study supervision: H.C. Reinhardt, P.-O. Frappart, A. Kleger

Acknowledgments

We are indebted to our patients, who provided primary material. We thank Alexandra Florin, Marion Müller, and Ursula Rommerscheidt-Fuß from the Institute of Pathology, University Hospital Cologne, for their outstanding technical support. We also thank Ralf Köhntop, Claudia Ruhland, Kristina Diepold, and Ulrike Mayr-Beyrle for technical assistance, and Tim Eiseler, Anett Illing, and Albrecht Neese for helpful scientific exchange.

Grant Support

This study was funded by the Deutsche Forschungsgemeinschaft (DFG, K.L. 2544/1-1 and 1-2), the Forschungskern SyStaR, the BIU (Böhringer Ingelheim), the NDIMED-Verbund PancChip, the Else-Kröner-Fresenius Stiftung (2011_A200), the Else-Kröner-Fresenius Memorial funding and Fritz-Thyssen Foundation (2015-00363), the Deutsche Krebshilfe (111879) to A. Kleger. A. Kleger is indebted to the Baden-Württemberg Stiftung for the financial support of this research project by the Eliteprogramme for Postdocs. L. Perkhofer is funded by the Else Kröner-Forschungskolleg Ulm. This work was supported by, the Deutsche Forschungsgemeinschaft (AZ.96 1-3) to N. Azoitei, the Deutsche Forschungsgemeinschaft (KFO-286), the Volkswagenstiftung (Lichtenberg Program), the Bundesministerium für Bildung und Forschung (SMOOSE), the German federal state North Rhine Westphalia (NRW) as part of the EFRE initiative (grant LS-1-1-030a), the Else Kröner-Fresenius Stiftung (EKFS-2014-A06) and the Deutsche Krebshilfe (111724) to H.C. Reinhardt. L. Wiesmüller and M. Ihle were supported by the Deutsche Forschungsgemeinschaft (B03 in the Research Training Group 2254 "Heterogeneity and evolution in solid tumors HEIST") and S. Hampp by a PhD fellowship of the DFG Graduate School of Molecular Medicine at Ulm University.

The costs of publication of this article were defrayed in part by the payment of page charges. This article must therefore be hereby marked *advertisement* in accordance with 18 U.S.C. Section 1734 solely to indicate this fact.

Received March 2, 2017; revised March 10, 2017; accepted August 3, 2017; published OnlineFirst August 8, 2017.

References

1. Quante AS, Ming C, Rottmann M, Engel J, Boeck S, Heinemann V, et al. Projections of cancer incidence and cancer-related deaths in Germany by 2020 and 2030. Cancer Med 2016;5:2649–56.
2. Waddell N, Pajic M, Patch AM, Chang DK, Kassahn KS, Bailey P, et al. Whole genomes redefine the mutational landscape of pancreatic cancer. Nature 2015;518:495–501.
3. Yachida S, Jones S, Bozic I, Antal T, Leary R, Fu B, et al. Distant metastasis occurs late during the genetic evolution of pancreatic cancer. Nature 2010;467:1114–7.
4. Notta F, Chan-Seng-Yue M, Lemire M, Li Y, Wilson GW, Connor AA, et al. A renewed model of pancreatic cancer evolution based on genomic rearrangement patterns. Nature 2016;538:378–82.
5. Roberts NJ, Norris AL, Petersen GM, Bondy ML, Brand R, Gallinger S, et al. Whole genome sequencing defines the genetic heterogeneity of familial pancreatic cancer. Cancer Discov 2016;6:166–75.
6. Cremona CA, Behrens A. ATM signalling and cancer. Oncogene 2014;33:3351–60.
7. Reinhardt HC, Yaffe MB. Phospho-Ser/Thr-binding domains: navigating the cell cycle and DNA damage response. Nat Rev Mol Cell Biol 2013;14:563–80.
8. Russell R, Perkhofer L, Liebau S, Lin Q, Lechel A, Feld FM, et al. Loss of ATM accelerates pancreatic cancer formation and epithelial-mesenchymal transition. Nat Commun 2015;6:7677.
9. Grigaravicius P, Kaminska E, Hubner CA, McKinnon PJ, von Deimling A, Frappart PO. Rint1 inactivation triggers genomic instability, ER stress and autophagy inhibition in the brain. Cell Death Differ 2016;23:454–68.
10. Schrock E, du Manoir S, Veldman T, Schoell B, Wienberg J, Ferguson-Smith MA, et al. Multicolor spectral karyotyping of human chromosomes. Science 1996;273:494–7.
11. Liyanage M, Coleman A, du Manoir S, Veldman T, McCormack S, Dickson RB, et al. Multicolour spectral karyotyping of mouse chromosomes. Nat Genet 1996;14:312–5.
12. Hampp S, Kiessling T, Buechle K, Mansilla SF, Thomale J, Rall M, et al. DNA damage tolerance pathway involving DNA polymerase iota and the tumor suppressor p53 regulates DNA replication fork progression. Proc Natl Acad Sci U S A 2016;113:E4311–9.
13. Bang YJ, Im SA, Lee KW, Cho JY, Song EK, Lee KH, et al. Randomized, double-blind phase II trial with prospective classification by ATM protein level to evaluate the efficacy and tolerability of olaparib plus paclitaxel in patients with recurrent or metastatic gastric cancer. J Clin Oncol 2015;33:3858–65.
14. Shiloh Y, Ziv Y. The ATM protein kinase: regulating the cellular response to genotoxic stress, and more. Nat Rev Mol Cell Biol 2013;14:197–210.
15. Turinetto V, Giachino C. Multiple facets of histone variant H2AX: a DNA double-strand-break marker with several biological functions. Nucleic Acids Res 2015;43:2489–98.
16. Reinhardt HC, Yaffe MB. Kinases that control the cell cycle in response to DNA damage: Chk1, Chk2, and MK2. Curr Opin Cell Biol 2009;21:245–55.

17. Ward IM, Chen J. Histone H2AX is phosphorylated in an ATR-dependent manner in response to replicational stress. J Biol Chem 2001; 276:47759–62.
18. Caldwell ME, DeNicola GM, Martins CP, Jacobetz MA, Maitra A, Hruban RH, et al. Cellular features of senescence during the evolution of human and murine ductal pancreatic cancer. Oncogene 2012;31:1599–608.
19. Kleger A, Perkhofer L, Seufferlein T. Smarter drugs emerging in pancreatic cancer therapy. Ann Oncol 2014;25:1260–70.
20. Pommier Y, O'Connor MJ, de Bono J. Laying a trap to kill cancer cells: PARP inhibitors and their mechanisms of action. Sci Transl Med 2016;8: 362ps17.
21. De Vos M, Schreiber V, Dantzer F. The diverse roles and clinical relevance of PARPs in DNA damage repair: current state of the art. Biochem Pharmacol 2012;84:137–46.
22. Aly A, Ganesan S. BRCA1, PARP, and 53BP1: conditional synthetic lethality and synthetic viability. J Mol Cell Biol 2011;3:66–74.
23. Keimling M, Volcic M, Csernok A, Wieland B, Dork T, Wiesmuller L. Functional characterization connects individual patient mutations in ataxia telangiectasia mutated (ATM) with dysfunction of specific DNA double-strand break-repair signaling pathways. FASEB J 2011;25:3849–60.
24. Neelsen KJ, Lopes M. Replication fork reversal in eukaryotes: from dead end to dynamic response. Nat Rev Mol Cell Biol 2015;16:207–20.
25. Tomimatsu N, Mukherjee B, Burma S. Distinct roles of ATR and DNA-PKcs in triggering DNA damage responses in ATM-deficient cells. EMBO Rep 2009;10:629–35.
26. Riabinska A, Daheim M, Herter-Sprie GS, Winkler J, Fritz C, Hallek M, et al. Therapeutic targeting of a robust non-oncogene addiction to PRKDC in ATM-defective tumors. Sci Transl Med 2013;5:189ra78.
27. Witkiewicz AK, McMillan EA, Balaji U, Baek G, Lin WC, Mansour J, et al. Whole-exome sequencing of pancreatic cancer defines genetic diversity and therapeutic targets. Nat Commun 2015;6:6744.
28. Biankin AV, Waddell N, Kassahn KS, Gingras MC, Muthuswamy LB, Johns AL, et al. Pancreatic cancer genomes reveal aberrations in axon guidance pathway genes. Nature 2012;491:399–405.
29. Bailey P, Chang DK, Nones K, Johns AL, Patch AM, Gingras MC, et al. Genomic analyses identify molecular subtypes of pancreatic cancer. Nature 2016;531:47–52.
30. Rabenau K, Hofstatter E. DNA damage repair and the emerging role of Poly (ADP-ribose) polymerase inhibition in cancer therapeutics. Clin Ther 2016;38:1577–88.
31. Caiola E, Salles D, Frapolli R, Lupi M, Rotella G, Ronchi A, et al. Base excision repair-mediated resistance to cisplatin in KRAS(G12C) mutant NSCLC cells. Oncotarget 2015;6:30072–87.
32. Rausch T, Jones DT, Zapatka M, Stutz AM, Zichner T, Weischenfeldt J, et al. Genome sequencing of pediatric medulloblastoma links catastrophic DNA rearrangements with TP53 mutations. Cell 2012;148:59–71.
33. Chen CH, Lin DS, Cheng CW, Lin CJ, Lo YK, Yen CC, et al. Cdc6 cooperates with c-Myc to promote genome instability and epithelial to mesenchymal transition EMT in zebrafish. Oncotarget 2014; 5:6300–11.
34. Comaills V, Kabeche L, Morris R, Buisson R, Yu M, Madden MW, et al. Genomic instability is induced by persistent proliferation of cells undergoing epithelial-to-mesenchymal transition. Cell Rep 2016;17: 2632–47.
35. Erkan M, Adler G, Apte MV, Bachem MG, Buchholz M, Detlefsen S, et al. StellaTUM: current consensus and discussion on pancreatic stellate cell research. Gut 2012;61:172–8.
36. Sistigu A, Manic G, Obrist F, Vitale I. Trial watch - inhibiting PARP enzymes for anticancer therapy. Mol Cell Oncol 2016;3:e1053594.
37. Tong WM, Hande MP, Lansdorp PM, Wang ZQ. DNA strand break-sensing molecule poly(ADP-Ribose) polymerase cooperates with p53 in telomere function, chromosome stability, and tumor suppression. Mol Cell Biol 2001;21:4046–54.
38. Nicolas L, Martinez C, Baro C, Rodriguez M, Baroja-Mazo A, Sole F, et al. Loss of poly(ADP-ribose) polymerase-2 leads to rapid development of spontaneous T-cell lymphomas in p53-deficient mice. Oncogene 2010;29:2877–83.
39. Weston VJ, Oldreive CE, Skowronska A, Oscier DG, Pratt G, Dyer MJ, et al. The PARP inhibitor olaparib induces significant killing of ATM-deficient lymphoid tumor cells *in vitro* and *in vivo*. Blood 2010; 116:4578–87.
40. Murai J, Huang SY, Das BB, Renaud A, Zhang Y, Doroshow JH, et al. Trapping of PARP1 and PARP2 by clinical PARP inhibitors. Cancer Res 2012;72:5588–99.
41. Schmitt A, Knittel G, Welcker D, Yang TP, George J, Nowak M, et al. ATM deficiency is associated with sensitivity to PARP1 and ATR inhibitors in lung adenocarcinoma. Cancer Res 2017;77:3040–56.
42. Jaspers JE, Kersbergen A, Boon U, Sol W, van Deemter L, Zander SA, et al. Loss of 53BP1 causes PARP inhibitor resistance in Brca1-mutated mouse mammary tumors. Cancer Discov 2013;3:68–81.
43. Edwards SL, Brough R, Lord CJ, Natrajan R, Vatcheva R, Levine DA, et al. Resistance to therapy caused by intragenic deletion in BRCA2. Nature 2008;451:1111–5.
44. Lupo B, Trusolino L. Inhibition of poly(ADP-ribosyl)ation in cancer: old and new paradigms revisited. Biochim Biophys Acta 2014;1846: 201–15.
45. Buisson R, Boisvert JL, Benes CH, Zou L. Distinct but concerted roles of ATR, DNA-PK, and Chk1 in countering replication stress during S phase. Mol Cell 2015;59:1011–24.
46. Jiang H, Reinhardt HC, Bartkova J, Tommiska J, Blomqvist C, Nevanlinna H, et al. The combined status of ATM and p53 link tumor development with therapeutic response. Genes Dev 2009;23:1895–909.